AGU PUBLICATIONS

JGR

Journal of Geophysical Research: Solid Earth

RESEARCH ARTICLE

10.1002/2013JB010889

Key Points:
- A new GPS velocity field for Fennoscandia based on more stations and more data
- Plate tectonics and reference frame issues might bias results from GIA models
- New approach to compare observations and models in a consistent reference frame

Supporting Information:
- Readme
- Table S1
- Figure S1

Correspondence to:
H. P. Kierulf,
halfdan.kierulf@kartverket.no

Citation:
Kierulf, H. P., H. Steffen, M. J. R. Simpson, M. Lidberg, P. Wu, and H. Wang (2014), A GPS velocity field for Fennoscandia and a consistent comparison to glacial isostatic adjustment models, *J. Geophys. Res. Solid Earth*, *119*, 6613–6629, doi:10.1002/2013JB010889.

Received 23 DEC 2013
Accepted 14 JUL 2014
Accepted article online 18 JUL 2014
Published online 14 AUG 2014

A GPS velocity field for Fennoscandia and a consistent comparison to glacial isostatic adjustment models

Halfdan Pascal Kierulf[1,2], Holger Steffen[3], Matthew James Ross Simpson[1], Martin Lidberg[3], Patrick Wu[4], and Hansheng Wang[5]

[1]Geodetic Institute, Norwegian Mapping Authority, Hønefoss, Norway, [2]Department of Geosciences, University of Oslo, Oslo, Norway, [3]Lantmäteriet, Gävle, Sweden, [4]Department of Geosciences, University of Hong Kong, Hong Kong, Hong Kong, [5]State Key Laboratory of Geodesy and Earth's Dynamics, Institute of Geodesy and Geophysics, Chinese Academy of Sciences, Wuhan, China

Abstract In Fennoscandia, the process of Glacial Isostatic Adjustment (GIA) drives ongoing crustal deformation. Crustal velocities from GPS observations have proved to be a useful tool in constraining GIA models. However, reference frame uncertainties, plate tectonics, intraplate deformations as well as other geophysical processes contaminate the results. Former studies have shown that different International Terrestrial Reference Frames have large discrepancies, especially in the vertical component, which hamper geophysical interpretation. We present new velocity estimates for the Fennoscandian and North European GPS network. Our GPS velocity field is directly realized in a GIA reference frame. Using this method (named the GIA frame approach) we are able to constrain GIA models with minimal influence of errors in the reference frame or biasing signals from plate tectonics. The drawbacks are more degrees of freedom that might mask real but unmodeled signals. Monte Carlo tests suggest that our approach is robust at the 97% level in terms of correctly separating different models of ice history but, depending on deformation patterns, the identified Earth model may be slightly biased in up to 39% of cases. We compare our results to different one- and three-dimensional GIA models employing different global ice-load histories. The GIA models generally provide good fit to the data but there are still significant discrepancies in some areas. We suggest that these differences are mainly related to inaccuracies in the ice models and/or lateral inhomogeneities in the Earth structure under Fennoscandia. Thus, GIA models still need to be improved, but the GIA frame approach provides a base for further improvements.

1. Introduction

Owing to different geophysical processes, the Earth's crust is deforming on different temporal and spatial scales. In Fennoscandia, the ongoing relaxation of the Earth in response to past ice mass loss (termed Glacial Isostatic Adjustment (GIA), see *Steffen and Wu* [2011], for an overview) is, together with plate tectonics, the dominant source of crustal deformations. Observations from Global Navigation Satellite System (GNSS) networks in Fennoscandia have provided means to establish a precise velocity field for the region and a powerful tool for the study of geophysical processes and especially GIA (Note: We are only using signals from Global Positioning System (GPS) satellites and not the other GNSS satellites in this study. We therefore use the term GPS in the rest of this manuscript). The GPS observations show two main features. First, a pattern of crustal uplift with highest rates (~10 mm/yr at the center of uplift) [*Milne et al.*, 2001] corresponding to areas of thickest ice during the last glacial maximum (~21,000 years ago). Uplift rates decrease with distance from the maximum ice load. Second, horizontal movements indicate a regional deformation characterized by an outward spreading from the uplift center.

One of the main uses of the GPS-derived velocity field is to constrain GIA models [*Steffen and Wu*, 2011]. However, a major issue is how one can first separate the observable GIA signal from other measurable geophysical processes before making any comparisons to a GIA model. For example, processes such as plate tectonics [*Argus et al.*, 2011], neotectonic motions [*Olesen et al.*, 2013], and/or the elastic response to hydrological loading [*van Dam et al.*, 2001; *Wang et al.*, 2013] and present-day ice mass variations [*Khan et al.*, 2007; *Kierulf et al.*, 2009] can mask the GIA signal.

Past modeling studies have shown that ongoing GIA in North America [see *Mitrovica et al.*, 1994] and rotational effects associated with GIA [see, e.g., *Milne et al.*, 2004] produce a relatively uniform and not

insignificant signal of solid Earth motion over Europe. These "far field" GIA signals in the horizontal motion are impossible to separate from plate tectonics with GPS measurements alone. Hence, earlier studies have only used horizontal motions to a limited extent for constraining GIA models. However, GIA horizontal velocities might give valuable constraints on the lateral structures of the lithosphere and mantle [*Milne et al.*, 2004; *Steffen et al.*, 2006, 2007; *Steffen and Wu*, 2014].

Separation of the plate tectonic motion and the GIA signal from the observed GPS signal in Fennoscandia can be attempted in several ways. In *Johansson et al.* [2002] the horizontal velocities were realized in a reference frame comoving with the Eurasian plate. This comoving plate was determined by including only stations not affected by horizontal GIA. This velocity field was used in *Milne et al.* [2001] to constrain GIA models. *Kierulf et al.* [2003] subtracted the GIA signal from the GPS observations before estimating plate motion. Based on the GIA model from *Milne et al.* [2001], *Lidberg et al.* [2007] solved for an additional rigid rotation before comparing GPS results with the GIA models, whereas *Hill et al.* [2010] included transformation parameters in the observation equation between observations and their GIA model to account for possible reference frame problems. *Kierulf et al.* [2012] just assumed the motion of rigid Eurasia as realized by *Boucher and Altamimi* [2011] as representative for the plate tectonic motion of Eurasia.

A similar issue and equally important is the influence of the reference frame. A GPS-derived velocity field is normally realized in a predefined reference frame like the International Terrestrial Reference Frame 2008 (ITRF2008) using a so-called 14-parameter similarity transformation [*Altamimi et al.*, 2011]. However, if the reference frame is not appropriate for the geophysical process one is interested in, then one's interpretation of the results will be wrong. Indeed, unsolved problems related to reference frames and plate tectonics potentially bias the outcome of comparisons between observations and GIA models.

A reference frame like ITRF2008 is not necessarily the right frame to describe a geophysical process like GIA. ITRF2008 is a global reference frame with its theoretical origin at the Earth's center of mass (CM) (including oceans and atmosphere) [*Altamimi et al.*, 2011; *Blewitt*, 2003]. However, as GIA is a process mainly driven by the solid Earth, it might be better described in a center of Earth (CE) reference frame where the atmosphere and ocean are omitted [*Argus*, 2007, 2012; *Blewitt*, 2003].

Differences between the various ITRFs have been discussed extensively in several papers [e.g., *Argus*, 2007, 2012; *Teferle et al.*, 2009; *Lidberg et al.*, 2010; *Altamimi et al.*, 2011]. The newest (and most accurate) reference frame ITRF2008 is in close agreement with the previous one, ITRF2005, but differs from the earlier ITRF2000 mainly because of obsolete models in the analysis of ITRF2000 and shorter series. In Fennoscandia the differences between ITRF2000 and ITRF2008, which are based on the scale and translation parameters [*Altamimi et al.*, 2007, 2011], depend on the latitude and can reach the 1 mm/yr level both in the north and height component. *Wu et al.* [2011] found that ITRF2008 is consistent with CM at the 0.2 mm/yr level. *Argus* [2007], noting large differences in ITRF2000/ITRF2005, argued though that Earth's reference frame should be defined with the tightly constrained velocity of CE.

In this paper we present a new, extended, and updated GPS velocity field for Fennoscandia and northern Europe. In our analysis we compare the velocity field to a number of different GIA models. Here we use a new approach where the influence of plate tectonics and/or the reference frame is reduced to a minimum. The idea is to realize our GPS results directly in the reference frame given by the different GIA models and then evaluate the different GIA models in their own reference frame. The aim of this paper is to show that this approach ensures that biases in the reference frame or tectonic model do not degrade the results. Furthermore, we will show that the new approach provides a useful tool to separate plate tectonic and GIA signals.

In the next section, we describe the GPS network and the analysis of the data, this is followed by an overview of GIA models used. In section 4, we introduce our GIA frame approach. The results are presented in section 5. In section 6, the implications of our findings on plate tectonics and for reference frame realization are presented. In section 7, the GIA frame approach is tested and compared with traditional approaches. We test the robustness of our method by using Monte Carlo simulations in section 8. This is followed by the discussion. We summarize our findings in section 10.

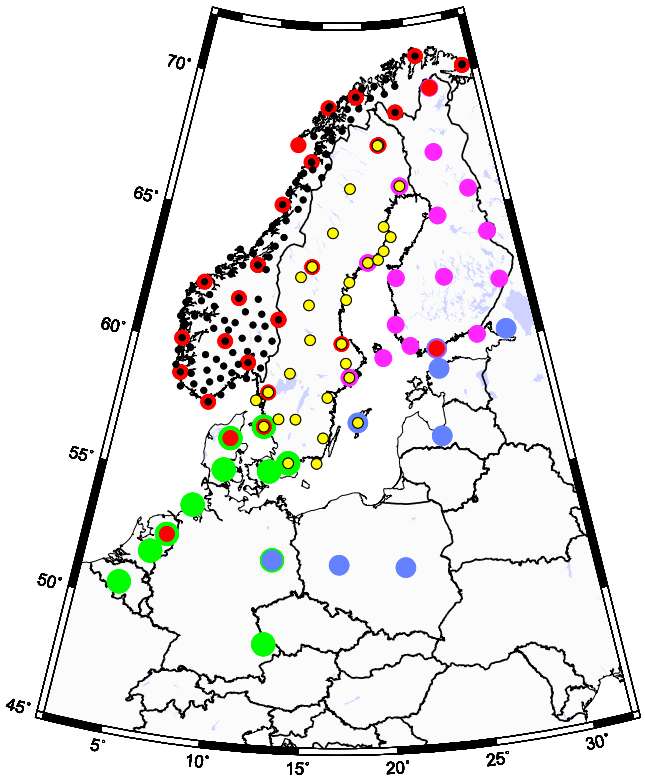

Figure 1. Overview of the GPS network used in this study. The different subnetworks used in the analysis are color-coded with circles of different sizes. Circles with several colors are used in several subnetworks and used to combine the different solutions. The scales are degrees latitude and longitude.

2. GPS Network and Analysis

The establishment of permanent GPS networks in the Nordic countries (Norway, Sweden, Finland, and Denmark) began in the early 1990s. A dense network exists in the region today, which is used for both geodynamic and geophysical studies. Many GIA-related GPS investigations have been completed under the Baseline Inferences for Fennoscandian Rebound Observations, Sea level, and Tectonics (BIFROST) project [*Scherneck et al.*, 1998]. Deformation rates from the BIFROST network have been published regularly [e.g., *Scherneck et al.*, 1998; *Milne et al.*, 2001; *Johansson et al.*, 2002; *Lidberg et al.*, 2007, 2010], largely incorporating Swedish and Finnish stations and also some Norwegian and North European stations. In *Kierulf et al.* [2012], velocities for all GPS stations in Norway with more than 3 years of data were published. In this work we include permanent Fennoscandian stations which have more than 3 years of data (see *Kierulf et al.* [2012], for a discussion of the relation between time series length and accuracy). In addition to these stations, a number of good quality sites from northern Europe are included. In total, we have 150 stations (see Figure 1).

In this study, we use the scientific GPS analysis software GAMIT/GLOBK [*Herring et al.*, 2011] to derive daily results for the permanent GPS stations in the study area. This software makes use of the so-called Double Difference (DD) approach, where a network of GPS stations is analyzed in a single adjustment. A least-square adjustment is used for the parameter estimation. This implies that parameters which vary with time, for example, the troposphere, have to be estimated as piecewise linear parameters. The atmospheric zenith delay is estimated with a 2-hourly piecewise linear model together with a daily troposphere gradient. Vienna Mapping Function (VMF1) [*Boehm et al.*, 2006] is used to model the hydrostatic and wet tropospheric delay. Ocean-loading coefficients are taken from the FES2004 model [*Scherneck*, 1991] and corrected for center of mass variations. Atmospheric loading and hydrological loading are not modeled in this analysis. The igs05.atx are employed to model the phase center variations and offsets. Observations with an elevation angle below 10° are removed from the analysis. The orbits are solved in the analysis with the IGS final orbits as a priori input.

Our network is divided into six subnetworks which are analyzed independently and then combined to a daily network including all stations. The subnetworks are highlighted color-coded in Figure 1. To ensure a good realization of our network in the global reference frame, global solutions from Massachusetts Institute of Technology (MIT) are included. The daily combined network is combined to a loosely constrained multiyear solution. That is, none of the station coordinates/velocities have a priori constraints that distort the internal consistency of the solution. The loosely constrained solution has no geophysical meaning before it is transformed to some appropriate reference frame. All the combinations are performed using GLOBK [*Herring et al.*, 2011]. As MIT used the igs08.atx phase center variations model after 18 April 2011, the problem with inconsistent antenna model parameters is mitigated by including scale parameters when combining the different subnetworks.

Table 1. Overview of GIA Models Used in This Study[a]

Name	Method	Ice Model	LT (km)	UM (10^{20} Pa s)	LM (10^{22} Pa s)	Number of Models
KL98-NMM	NMM	KL98	60–160	0.1–40	0.1–10	1089
ICE-5G-NMM	NMM	ICE-5G	60–160	0.1–40	0.1–10	1089
KL98-FEM	FEM	KL98	140	3D based on *Grand et al.* [1997] tomography model		1
ICE-5G-FEM	FEM	ICE-5G	140	3D based on *Grand et al.* [1997] tomography model		1
ICE-4G-FEM	FEM	ICE-4G	115	3D based on S20A tomography model [*Ekström and Dziewonski*, 1998]		1

[a]NMM: Normal mode method; FEM: Finite-element method; LT: Lithospheric thickness; UM: Upper-mantle viscosity; and LM: Lower-mantle viscosity.

GPS results are correlated both spatially and temporally. This has divided the geodetic community into two groups [*King et al.*, 2010]. One group neglects the spatial correlation and thus time series for each site are regarded independently; the other group neglects the temporal correlation but keeps the covariance information produced in the GPS analysis. With an appropriate time series analysis [e.g., *Williams et al.*, 2004] the first approach gives realistic velocity uncertainties, but the covariance is unresolved. The other approach gives uncertainties for the individual stations that are too optimistic [*King et al.*, 2010] but with covariance information retained. The latter is mandatory for reference frame realization and is consequently applied in this paper. We have also included velocity uncertainties based on time series analysis using CATS [*Williams*, 2008], including a combination of white noise and flicker noise (see supporting information).

3. Glacial Isostatic Adjustment Models

In general, a GIA model can be described with an Earth model and a global ice model. Corresponding changes in the ocean mass due to ice buildup and melt are handled with the sea level equation [*Farrell and Clark*, 1976]. Both the calculated changing ocean mass changes and the ice load history from the model are applied as load in the Earth model. We employ two different types of GIA models (finite element and normal mode) together with three different global ice models, which are summarized in Table 1. The GIA models are consequently named according to their type and the ice model applied.

The first ice model, which we call KL98, has been used in former BIFROST studies [*Milne et al.*, 2001, 2004; *Lidberg et al.*, 2007]. The Fennoscandian ice history is taken from *Lambeck et al.* [1998], and the ice sheet histories in other parts of the world are represented by the ICE-3G model [*Tushingham and Peltier*, 1991]. The commonly used ICE-5G v1.2 global ice model [*Peltier*, 2004] is also tested. Finally, one GIA model in our analysis also employs the ICE-4G global ice model [*Peltier*, 1994, 1996].

The first type of GIA model consists of a one-dimensional (1D) Earth model and a dedicated ice model (KL98 or ICE-5G) and employs the normal mode method (NMM) [*Wu*, 1978]. The Earth model is spherically symmetric (thus 1D), compressible, with a Maxwell viscoelastic rheology and with migrating shorelines and rotational feedback included. In general, distinct parameters of three layers, lithospheric thickness of the first layer, upper mantle, and lower mantle viscosity, respectively, in the two layers below the lithosphere, are varied. An inviscid Earth's core follows as a lower boundary. This model approach is the same as that used in earlier BIFROST publications [*Milne et al.*, 2001, 2004; *Lidberg et al.*, 2007] or similar studies for Fennoscandia [*Steffen and Kaufmann*, 2005; *Zhao et al.*, 2012]. The values of the three parameters envelope reasonable values known from former GIA studies: studies based on GPS results yielded values for such laterally homogeneous models bracketing 90–120 km for lithospheric thickness, (3–10) $\times 10^{20}$ Pa s for upper mantle viscosity and (2–30) $\times 10^{21}$ Pa s for lower mantle viscosity [*Steffen and Wu*, 2011; *Zhao et al.*, 2012]. These values are also supported by studies employing relative sea level data for the whole Scandinavian area [e.g., *Lambeck et al.*, 1998; *Steffen and Kaufmann*, 2005]. Data sets based on tide gauges or space-based gravity observations indicate that higher lithospheric thicknesses of 150–160 km are possible, while mantle viscosities agree with the ones from GPS results [*Steffen and Wu*, 2011]. Regionally grouped relative sea level data, as well as selected tide gauge data also yielded lower lithospheric thicknesses of about 60–70 km [*Steffen and Wu*, 2011]. We therefore use the parameter ranges indicated in Table 1 in our NMM investigation to cover possible thickness and viscosity values.

The second type of GIA model employs the finite element method (FEM). Here we use a three-dimensional (3D), laterally varying, spherical, incompressible, Maxwell viscoelastic Earth model with migrating shorelines and rotational feedback and solving of the sea level equation. This model is based on the approach

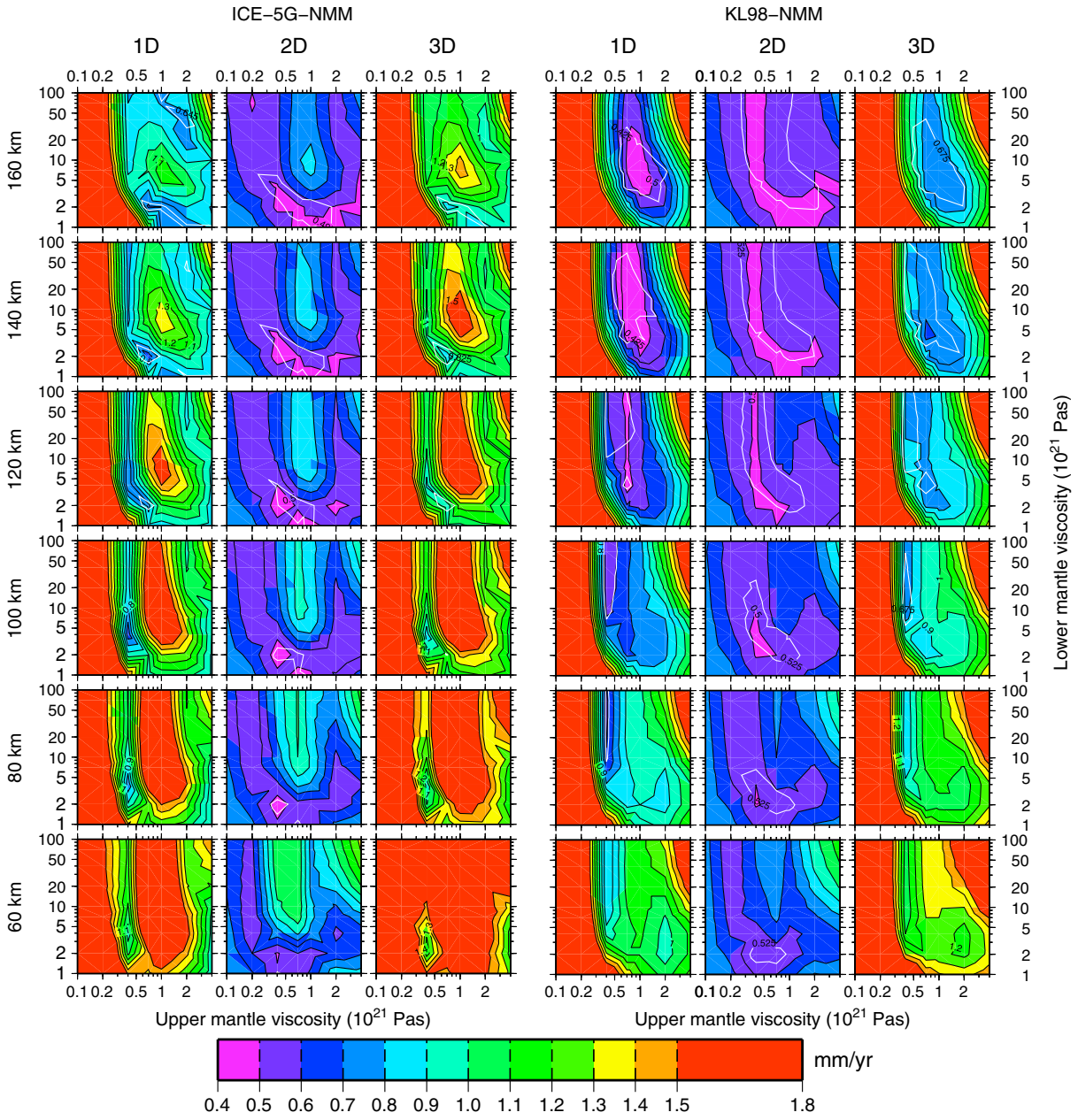

Figure 2. WRMS for ICE-5G-NMM and KL98-NMM models for different 1D Earth model parameters. All results are based on the differences between the observations and GIA model using the GIA frame approach. The white contour lines are the σ_1 confidence lines which enclose the GIA models that give (at σ_1 level) a similarly good fit to the observations as the best fitting GIA model. The columns are from left: up-component for ICE-5G-NMM, horizontal velocities for ICE-5G-NMM, 3D velocity field for ICE-5G-NMM, up-component for KL98-NMM, horizontal velocities for KL98-NMM, and 3D velocity field for KL98-NMM. Lithospheric thickness are from top 160 km, 140 km, 120 km, 100 km, 80 km, and 60 km.

described in *Wu* [2004]. With this model, it is possible to include lateral variations in lithospheric thickness and mantle viscosity. In this study, we keep the lithospheric thickness constant but apply different 3D viscosity structures based on seismic tomography models. The first seismic tomography model used is from *Grand et al.* [1997] and converted into a laterally varying mantle viscosity by a modified scaling relationship from *Ivins and Sammis* [1995]. A detailed description of the procedure can be found in *Wang et al.* [2008]. The background viscosity and lithospheric thickness of these models is taken from the best fitting 1D result for the respective ice models (KL98 or ICE-5G). The second seismic tomography model is from *Ekström and Dziewonski* [1998]. Here background viscosity and lithospheric thickness are from model RF3 by *Wang et al.* [2008]. Together with ICE-4G as ice load, this model fits different GIA observation simultaneously well [*Wang et al.*, 2008]. This GIA model is the only one in our analysis applying ICE-4G.

Table 2. One-Dimensional, 2D, and 3D WRMS for the Various Best Fitting Models

GIA Model	LT (km)	UM (10^{20} Pa s)	LM (10^{21} Pa s)	1D (mm/yr)	2D (mm/yr)	3D (mm/yr)
KL98-NMM	140	7	4	0.42	0.52	0.67
ICE-5G-NMM	140	7	2	0.64	0.49	0.82
KL98-FEM				0.63	0.60	0.90
ICE-5G-FEM				0.67	0.54	0.89
ICE-4G-FEM				1.65	0.57	1.74

4. The GIA Frame Approach

To give a GPS velocity field a physical meaning, it has to be realized in a reference frame. A reference frame is a list of station coordinates and velocities given relative to a given origin, with a given orientation and scale. A velocity field is often realized in a reference frame using a so-called 14-parameter similarity transformation [e.g., *Altamimi et al.*, 2011]. The parameters are the translation vector (three parameters), the rotation vector (three parameters), and the scale (one parameter) as well as the time derivative of these parameters. The reference frame can be regional, e.g., ETRF2000 [*Boucher and Altamimi*, 2011] or global, e.g., ITRF2008 [*Altamimi et al.*, 2011]. (ETRF2000 is a regional reference frame fixed to the stable part of the Eurasian Plate.)

The velocities in such a reference frame contain information from different geophysical processes. Since we use the velocity field to constrain the GIA models, the non-GIA contribution should be reduced to a minimum. Plate tectonic motion is the largest non-GIA signal that the observations need to be corrected for. Furthermore, a reference frame and a geophysical model do not necessarily have consistent origin, orientation and scale (see section 1). Contributions from other geophysical processes and inconsistencies in the reference frame will hamper the comparison between the velocity field and the GIA model.

To avoid the problems with plate tectonic and reference frame biases or uncertainties we use a new approach in this study. Each station in our GPS network has a position in a global realization of our GPS solution ($\vec{X}_i$). For a given GIA model we predict velocities for all the stations in our network ($\overrightarrow{v_i^{GIA}}$). These velocities are given relative to some origin, orientation and scale implicitly given by the GIA model. Hence, this list of positions and velocities define a reference frame consistent with the parameters in the GIA model. We name this reference frame a GIA reference frame. For each GIA model, we get a GIA reference frame.

Our GPS velocity field (the loosely constrained solution described in section 2), contains a velocity vector ($\overrightarrow{v_i^{GPS}}$) for each station. This velocity field is transformed to the GIA reference frame with a similarity transformation for each GIA model. Since scale rate and geocenter motion are strongly correlated for regional networks like ours, we cannot use the complete 14-parameter similarity transformation. We have therefore excluded the geocenter motion parameters from the transformation. The following observation equation is used for the transformations of the velocity field:

$$\overrightarrow{v_i^{GPS}} = \overrightarrow{v_i^{GIA}} + \begin{pmatrix} s & -\omega_3 & \omega_2 \\ \omega_3 & s & -\omega_1 \\ -\omega_2 & \omega_1 & s \end{pmatrix} \vec{X}_i + \overrightarrow{r_i^{GPS}}, \quad (1)$$

The unknowns are the three elements of the rotation matrix ($\omega_j, j \in 1,2,3$) and the scale rate parameter (s). The residual vector is $\overrightarrow{r_i^{GPS}}$. In the solution of the observation equation the complete covariance matrix of the velocities was included. The transformations were performed with the GAMIT/GLOBK routine GLORG, including iterative weighting and down weighting of the height component [*Herring et al.*, 2011].

The station residuals after the transformation are minimal in a least-square sense, and the transformed velocity field is as close as possible to the GIA reference frame without deforming the internal consistency of the GPS velocity field. The resulting realization of our GPS velocity field in the GIA reference frames are not hampered by possible reference frame biases or wrongly determined rigid plate tectonic motion. We name this approach *the GIA frame approach*. The observed velocities realized in the GIA reference frame are then $\overrightarrow{v_i^{GPS,GIA}} = \overrightarrow{v_i^{GIA}} + \overrightarrow{r_i^{GPS}}$.

The station residuals can then be used to evaluate the GIA model by some statistical measure, for instance, Weighted Root Mean Square (WRMS, see equation 2) or reduced χ^2. Although reduced χ^2 is a frequently

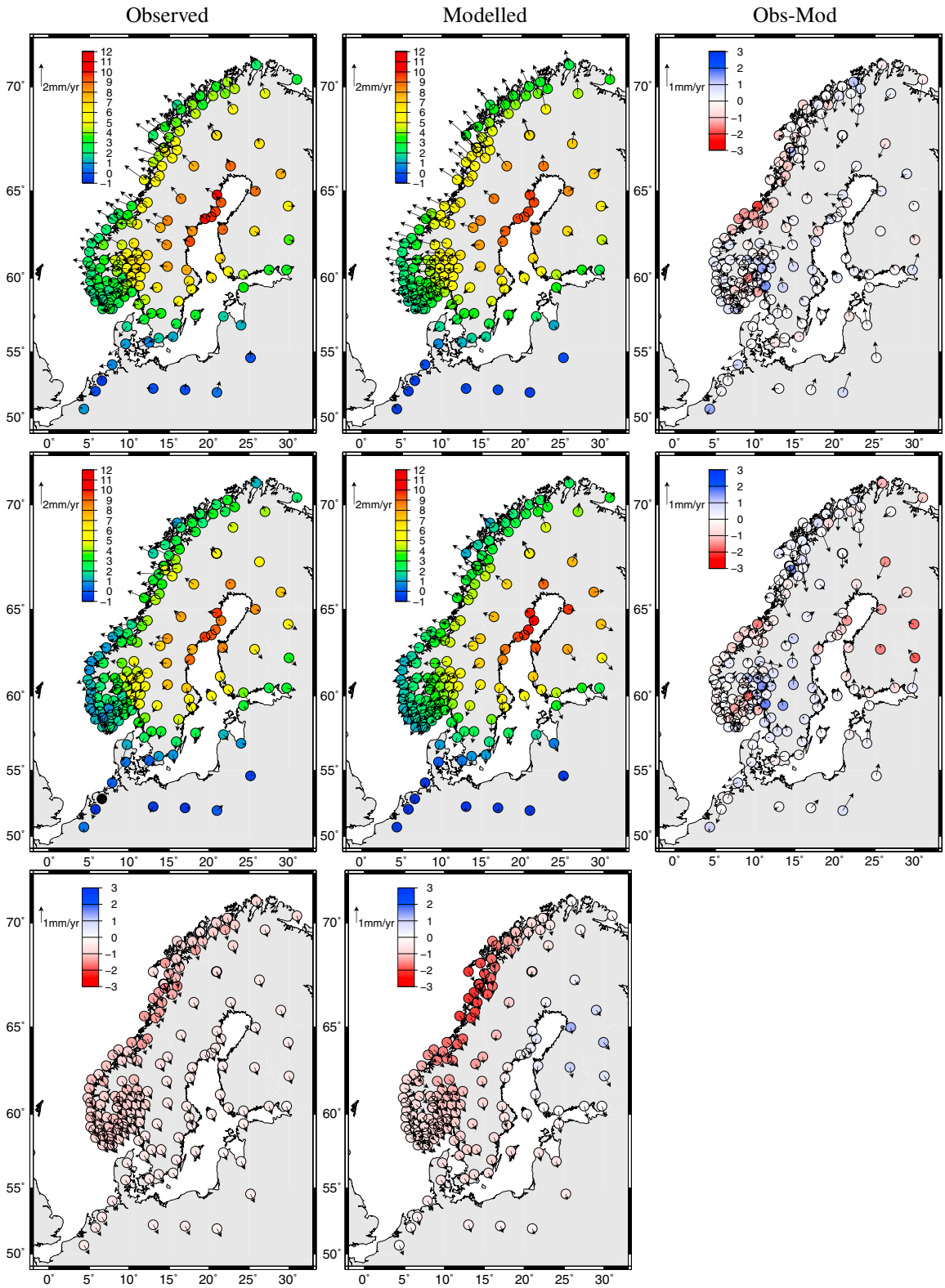

Figure 3. Comparison of observed velocity fields in the respective GIA model frame to the ones as determined with the best fitting 1D GIA models. (top, left) The observed velocity field in the GIA-model frame realization for the (top, middle) best fitting KL98-NMM 1D GIA model. (top, right) Difference between observations and model predictions. Middle row the same as top row, but for best fitting ICE-5G-NMM model. (bottom row) The difference between top and middle rows, i.e., (bottom, left) the difference in the GIA-reference frame between the best fitting GIA models for the ICE-5G and the KL98 ice model. (bottom, middle) The differences between the best fitting GIA model for the ICE-5G and the KL98 ice model.

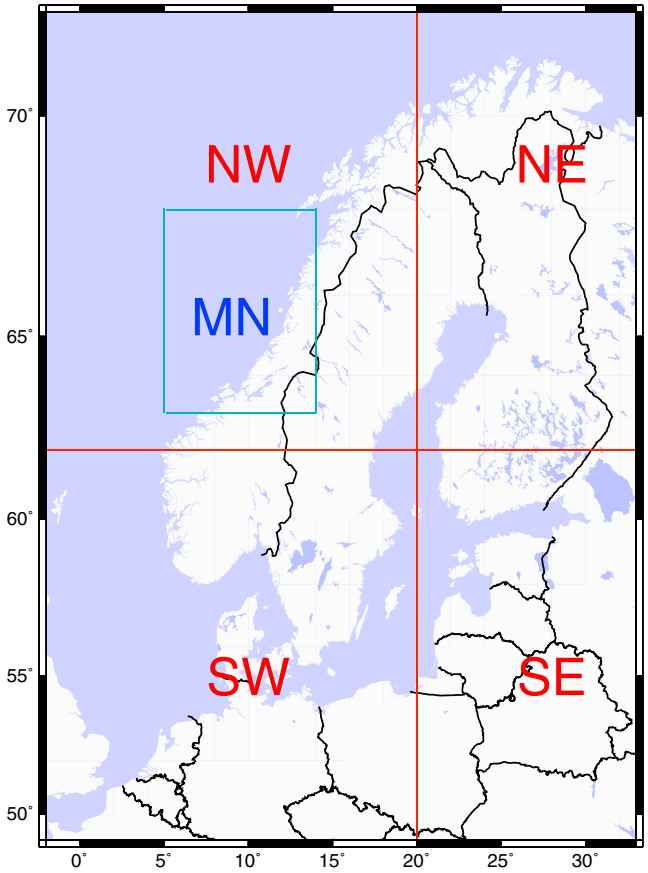

Figure 4. Different regions used in the quality assessment.

used test for assessing GIA models [e.g., *Milne et al.*, 2001], we use the WRMS since it gives a more intuitive understanding of the quality of the fit between models and observations. The two criteria give similar results when discriminating between geophysical models.

We will use 1D, 2D, and 3D WRMS in the GIA model validation, using the following formula:

$$\mathrm{WRMS} = \sqrt{\frac{\sum_{i=1}^{n}\left(\frac{r_i}{\sigma_i}\right)^2}{\sum_{i=1}^{n}\left(\frac{1}{\sigma_i}\right)^2}}, \qquad (2)$$

with σ_i as the corresponding uncertainty. In the 1D case, r_i is the difference between measured and modeled uplift for station *i*. For 2D (respectively 3D), r_i is the length of the vector difference between the observed and the modeled 2D horizontal (respectively full 3D) velocity vector. The $\sum_{i=1}^{n}$ is running through all the stations in the regional network (see Figure 1).

5. Results

Using the WRMS test we first determine the best fitting 1D model, i.e., the one with the lowest misfit between modeled and observed velocities. We show how goodness-of-fit varies with changes in the Earth model parameters in Figure 2. The best fitting models and their corresponding WRMS are identified and included in Table 2. In the horizontal component the fit is almost at the same level for both best fitting GIA models, while the fit in the vertical component has 18% lower WRMS for KL98-NMM.

In Figure 2, the σ_1 confidence is plotted as white contour lines. It encloses the area where the RMS of the GIA models relative to the best fitting GIA model are less than the WRMS of the observations relative to the best fitting model. The RMS can be found by using equation (2), but where r_i is the difference between predicted velocities from the various GIA models and the best fitting GIA model for station *i* and where the weights are uniform. Assuming that the WRMS of the observations relative to best fitting model is a measure of the uncertainties of the observations, the σ_1 confidence criteria is the same as the $\Psi = \sqrt{\frac{1}{N}\sum_{i=1}^{N}\left(\frac{r_i}{\sigma_i}\right)^2} \leq 1$ used in *Wu et al.* [2013]. The σ_1 contours in Figure 2 indicate that KL98-NMM models with lithospheric thickness between 120 km and 160 km, upper mantle viscosity between 0.5×10^{21} Pa s and 2×10^{21} Pa s and a lower mantle viscosity between 3×10^{21} Pa s and 5×10^{22} Pa s fit comparably well to the observations (at σ_1 level) as the best fitting model. For the ICE-5G-NMM the area of comparably well-fitting GIA models is narrower.

In Figure 3, the velocities of the best fitting GIA models, the corresponding GPS velocities, and the residuals are plotted. A visual inspection of Figure 3 indicates that, for ICE-5G-NMM, there are some discrepancies in the vertical component (color-coded dots) for stations in the northeast (62°–72°N and 20°–40°E). ICE-5G-NMM overpredicts uplift in this area. This is not seen for KL98-NMM. For mid-Norway, KL98-NMM overpredicts the uplift. To examine these discrepancies, we divide our network into several regional subnetworks: northeast, northwest, southeast, and southwest (NE, NW, SE, and SW in Figure 4). The WRMS are

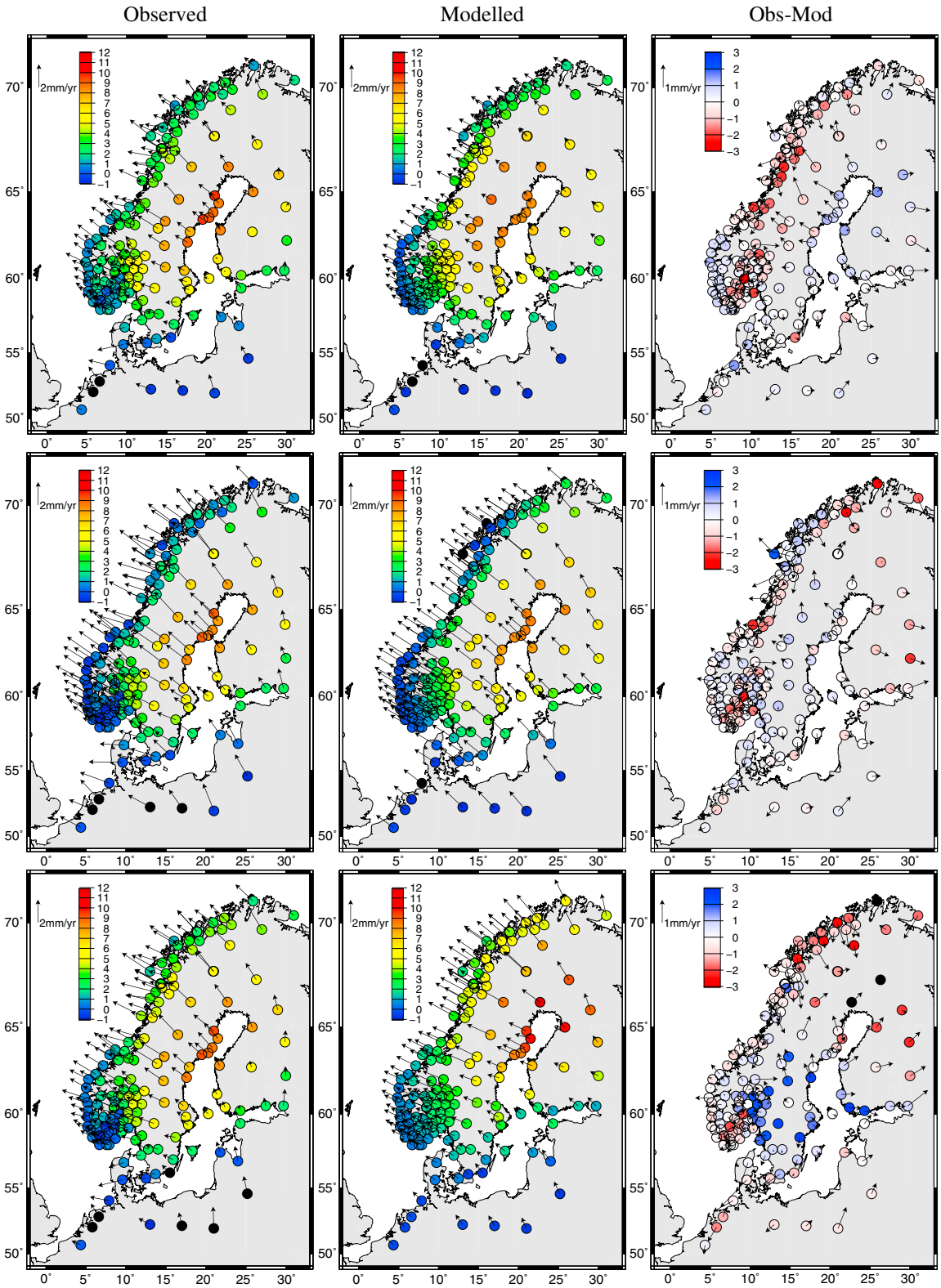

Figure 5. Same as Figure 3 but for 3D GIA models. (top) For KL98-FEM, (middle) for ICE-5G-FEM, and (bottom) for ICE-4G-FEM. (left column) Observed velocity fields are realized in the respective GIA-reference frame given by the GIA model.

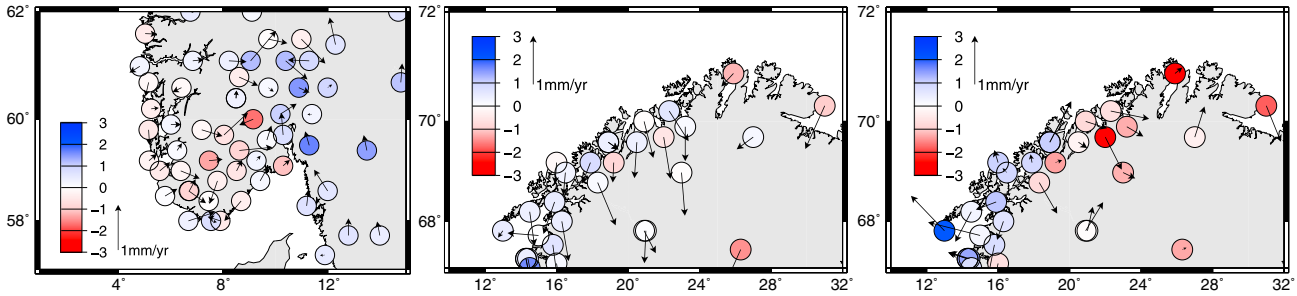

Figure 6. Local deformations. The panels show the difference between observations and GIA models (same as in Figures 3 (right) and 5, but limited to the (left) Southern Norway and (middle and right) Northern Fennoscandia). The GIA models are the best fitting 1D model for (left and middle) ICE-5G and the (right) 3D ICE-5G model.

computed for each region. In all regions except northeast, ICE-5G-NMM and KL98-NMM perform at the same level. In the northeast the WRMS of the up-component is 1.04 mm/yr for ICE-5G-NMM, more than twice the value of 0.41 mm/yr achieved with KL98-NMM. To examine the signal in mid-Norway (MN in Figure 4), an additional area reaching from 63° to 68°N and west of 14°E is tested. In this area the vertical WRMS for KL98-NMM is 1.20 mm/yr, while the corresponding value for ICE-5G-NMM is 0.60 mm/yr.

In Figure 5 the results for the three tested 3D GIA models are plotted, and their corresponding WRMS are included in Table 2. KL98-FEM and ICE-5G-FEM perform almost equally well. The 3D GIA models have generally higher WRMS than the best fitting 1D GIA models, leaving room for detailed future investigations. Especially, the vertical component for KL98-FEM is not at the level of the best fitting KL98-NMM model. The WRMS for the ICE-4G-FEM are the largest of the 3D models and, therefore, the ICE-4G performs relatively poorly in this test.

Although the 3D GIA models generally perform worse than the 1D model, there are two interesting exceptions. In the problematic northeast area for ICE-5G-NMM, ICE-5G-FEM performs better, and in mid-Norway, KL98-FEM performs better than KL98-NMM in the vertical component. In the northeast, where ICE-5G-NMM had large vertical residuals, ICE-5G-FEM shows a small improvement (vertical WRMS of 0.91 mm/yr instead of 1.04 mm/yr). In mid-Norway, where KL98-NMM overpredicts the uplift, KL98-FEM fits better by reducing the misfit by 25% (0.89 mm/yr instead of 1.20 mm/yr).

In Southeastern Norway (the area around Oslo), the measured uplift is larger than the predictions from the best fitting 1D model for both KL98 and ICE-5G. The horizontal residuals are also larger in this area (see Figure 6), indicating some unmodeled deformations, but no clear pattern is discernable. In the northernmost parts of Fennoscandia, relatively large horizontal residuals are found with the 1D models, while the vertical residuals are generally small (Figure 6); whereas for the 3D models, we find smaller horizontal residuals but an increase in the vertical residuals. A rigorous geophysical interpretation of these signals is an issue for further investigations.

In the supporting information we show velocity and uncertainty estimates from the GAMIT/GLOBK analysis (Note: The GAMIT/GLOBK analysis includes no temporal correlation, only white noise, but keeps the spatial covariance information from the GPS analysis). In addition, we include uncertainties based on time series analysis using CATS, where we assume a combination of white noise and flicker noise. See section 2 for more about the difference between the two approaches. The mean uncertainty in the north component using CATS is 5.3 times larger than the uncertainty from the GAMIT/GLOBK analysis. Corresponding numbers in the east and north components are 6.0 and 5.6, respectively.

6. Implications for Plate Tectonic and Reference Frames

We have, in this paper, realized our velocity field directly in the reference frames of the different GIA models (the GIA frame approach, see section 4), i.e., independently of a global reference frame. The transformation parameters between ITRF2008 and some selected GIA models are included in Table 3. Note: Only scale rate and rotation are included in the transformation between the ITRF2008 and our GIA-reference frames due to the correlation between scale rate and geocenter motion for a regional network like ours.

Table 3. Transformation Parameters From ITRF2008 to Different GIA Reference Frames[a]

Ice Model	RX (mas/yr)	RY (mas/yr)	RZ (mas/yr)	Scale Rate (mm/yr)
ICE-5G-NMM[b]	0.096 ± 0.015	0.530 ± 0.005	−0.731 ± 0.027	0.45 ± 0.10
KL98-NMM[b]	0.103 ± 0.012	0.515 ± 0.004	−0.742 ± 0.022	−0.19 ± 0.08
ICE-5G-FEM	0.136 ± 0.016	0.487 ± 0.006	−0.777 ± 0.030	1.20 ± 0.11
KL98-FEM	0.097 ± 0.016	0.499 ± 0.006	−0.792 ± 0.029	0.51 ± 0.11
ICE-4G-FEM	0.151 ± 0.031	0.508 ± 0.011	−0.705 ± 0.057	0.83 ± 0.21
BA11[c]	0.081 ± 0.021	0.490 ± 0.008	−0.792 ± 0.026	(−1.00)[d]
A12[e]	0.083 ± 0.08	0.534 ± 0.07	−0.750 ± 0.08	

[a]The covariance matrix is scaled with the factors between velocity estimates using a white noise plus flicker noise model and the full covariance found in section 2. Uncertainties are the 1 sigma confidence interval.
[b]The Earth model is the best fitting 1D Earth model.
[c]BA11 is the transformation from ITRF2008 to ETRF2000 [*Boucher and Altamimi*, 2011].
[d]The scale rate parameter is the resultant of scale rate and geocenter motion for a station at 60°N. It is the same as the difference between ITRF2008 and ITRF2000.
[e]A12 is the Eurasian plate rotation pole from *Altamimi et al.* [2012] (for 69 stations without GIA correction).

The three angular velocities reflect the plate tectonic motion of Eurasia relative to ITRF2008, without any contribution from the GIA signal predicted by the GIA model. The rigid rotation between ITRF2008 and ETRF2000 from *Boucher and Altamimi* [2011] and the Eurasian plate rotation pole from *Altamimi et al.* [2012] (for 69 stations without GIA correction) are also included in Table 3. We note a relatively good agreement, i.e., the rotations are consistent within the uncertainties shown in *Altamimi et al.* [2012]. However, the rigid rotation [*Boucher and Altamimi*, 2011] is based on GPS solely and contains signals attributable to GIA.

A scale rate parameter of approximately 0.075 ppb/yr (the scale rate transformation parameter from ITRF2008 to the best fitting ICE-5G-NMM model) indicates that vertical velocities in ITRF2008 are around 0.45 mm/yr smaller than the velocities predicted by the best fitting ICE-5G-NMM GIA model in Fennoscandia. For KL98-NMM the scale rate parameter is −0.030 ppb/yr (−0.19 mm/yr).

The scale rate parameter depends strongly on the Earth model. In Figure 7 the scale rate parameter for the transformation from ITRF2008 to the different ICE-5G GIA reference frames are plotted as function of Earth model parameter. The scale rate parameter varies ±0.5 ppb/yr which corresponds to ±3 mm/yr uplift on the Earth surface. Small perturbations of the mantle viscosity of our best fitting GIA models give large variations in the scale rate parameter. For this model the scale rate is 0.075 ppb/yr (0.45 mm/yr). A slight increase in the upper mantle viscosity to 1×10^{21} Pa s gives a scale factor of −0.011 ppb/yr (−0.07 mm/yr). When slightly decreasing the lower mantle viscosity to 1×10^{21} Pa s and keeping the upper mantle viscosity at

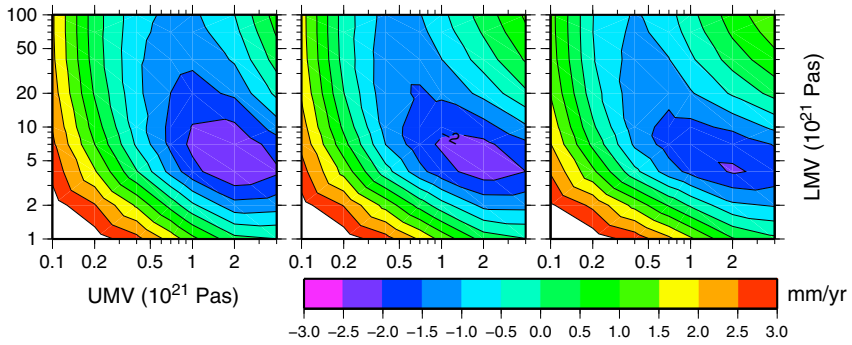

Figure 7. Scale rate parameter between ITRF2008 and ICE-5G-NMM GIA reference frames. The scale rate parameter is converted to equivalent uplift in mm/yr on the Earth surface. Lithospheric thickness is from left 60, 100, and 140 km. UMV is the upper mantle viscosity and LMV is the lower mantle viscosity.

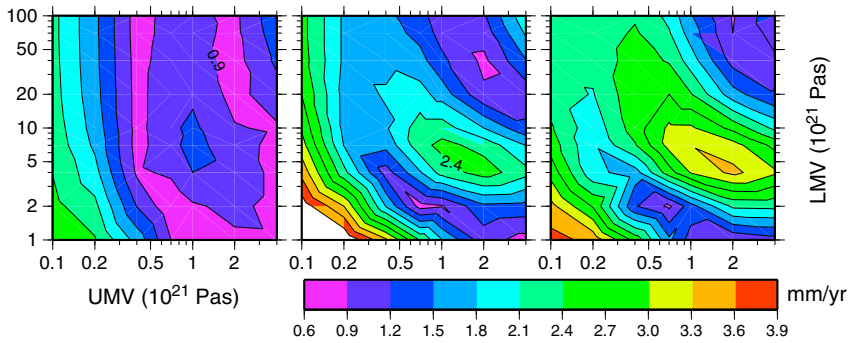

Figure 8. WRMS for the up component compared to the ICE-5G-NMM result. The lithospheric thickness is 140 km. (left) The results are based on the GIA frame approach. In the two other panels we have realized our velocity field in (middle) ITRF2008 and (right) ITRF2000. UMV is the upper mantle viscosity and LMV is the lower mantle viscosity.

7×10^{20} Pa s, the scale rate is 0.334 ppb/yr (2.12 mm/yr). A thicker or thinner lithosphere does not significantly affect the scale rate.

7. Fixing the Scale Rate and Rigid Rotation

To evaluate the GIA frame approach, we compare the method with results using the traditional method where the reference frame is fixed and a rigid rotation removed. In other words, we realize our velocity field in a predefined reference frame (e.g., ITRF2000 and ITRF2008) and remove the rigid rotation using parameters from earlier studies. Note: Since we do not solve for translation, the scale rate parameter will absorb the contribution of geocenter motion to the uplift. Due to the limited extent of our network, the spatial variations in the uplift from geocenter motion is negligible (less than 10% of the geocenter motion in the *Z* direction).

In this comparison we only use the ICE-5G-NMM models and restrict ourselves to a lithospheric thickness of 140 km. Results with KL98 and other lithospheric thickness give similar results but are not shown here. Figure 8 shows 1D WRMS fits between observations and GIA models. In Figure 8 (left), the WRMS using the GIA frame approach is shown. In Figure 8 (middle and right), our velocity field is realized in ITRF2008 and ITRF2000, respectively, and the WRMS is based on the differences between the uplift as realized in ITRF2008 (respectively ITRF2000) and the GIA models. When the reference frame is fixed, the WRMS value increases faster when the Earth viscosity parameters are varied from those of the best fitting model. The scale rate parameter can absorb a large fraction of the variations in the GIA models, when we are using the GIA frame approach. This implies that if we know the scale with sufficient precision, the constraints on the GIA model are much tighter. However, the accuracy of scale and geocenter rates in the global reference frame are questioned [e.g., *Argus*, 2012]. If the scale and geocenter in the reference frame are wrongly determined, the constraints on the GIA model are wrong. For instance, if we realize our GPS velocity field in ITRF2000, the best fitting GIA model will have a lithospheric thickness of 140 km, an upper mantle viscosity of 2×10^{21} Pa s and a lower mantle viscosity of 1×10^{23} Pa s. This is of high interest in GIA modeling as earlier inferences of lower mantle viscosity may have been biased by the reference frame.

In Figure 9, the 2D horizontal WRMS fit for various Earth models with 140 km lithospheric thickness is plotted. In Figure 9 (left), the GIA frame approach is used. In Figure 9 (middle), we remove the rigid rotation for ETRF2000 presented in *Boucher and Altamimi* [2011] (from here on named BA11), while in Figure 9 (right), we remove the *Altamimi et al.* [2012] rotation pole (69 stations without GIA correction, from here on named A12). When the rigid rotation is removed the WRMS value increases much faster when the Earth viscosity parameters are varied from the parameters of the best fitting GIA model. For the A12 rotation pole, the best fit is very close to the best fit found with the GIA frame approach, while BA11 gives the best fit for different Earth model parameters (upper mantle viscosity of 4×10^{20} Pa s and lower mantle viscosity of 7×10^{21} Pa s). This is not surprising since the A12 rotation agrees, within the uncertainties, with the rotation estimated between ITRF2008 and our best fit GIA model. Whereas, the BA11 rotation differs from the rotation between ITRF2008 and our best fit GIA model (i.e., they differ by approximately 2 sigma).

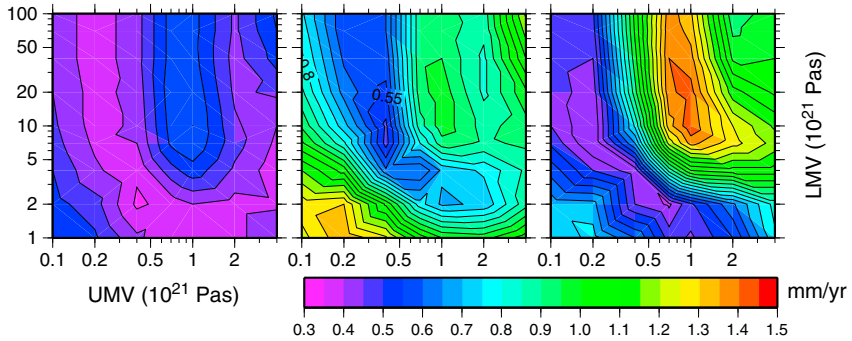

Figure 9. WRMS for the 2D horizontal component compared to the ICE-5G-NMM result. The lithospheric thickness is 140 km. (left) The results are based on the GIA frame approach. In the other panels, the rotation of Eurasia is assumed to be the same as in (middle) *Boucher and Altamimi* [2011] and (right) *Altamimi et al.* [2012]. UMV is the upper mantle viscosity and LMV is the lower mantle viscosity.

Of course, if the rigid rotation associated with plate motion is perfectly known, then this gives a highly valuable constraint when determining our best fitting GIA model. However, if the rigid rotation parameters are incorrect, then the comparison between the observations and the GIA model will also be incorrect. This, in turn, means our geophysical interpretation of the results will be wrong.

8. Validation of the GIA Frame Approach

To evaluate the GIA frame approach, we have performed three different tests based on Monte Carlo simulations. In these tests we examine three different velocity fields, and in each case we assume this to be the "true" velocity field for Fennoscandia. The three tests reflect different assumptions about the geophysical processes operating in Fennoscandia (see the paragraph below). Using the Monte Carlo method, realistic random velocity biases were added to the "true" velocity fields to give a new simulated GPS field. The velocity biases come from a random sample of the normal distribution with the standard deviation given by a site- and component-dependent realistic standard deviation. These standard deviations were computed using the time series analysis software CATS [*Williams*, 2008], where a combination of white noise and flicker noise was assumed. In addition, a rate bias was added to the geocenter of the reference frame. The geocenter rate biases come from a random sample of normal distribution with standard deviation equal to the geocenter motion values proposed in *Argus* [2012] (scale rate and rigid rotation biases were not added since they would have been completely absorbed in the transformation parameters). The deformed velocity field was then transformed to a set of 250 different GIA reference frames using the GIA frame approach. Lithospheric thickness was varied between 120 km and 160 km, upper mantle viscosity between 2×10^{20} Pa s and 2×10^{21} Pa s, and lower mantle viscosity between 1×10^{21} Pa s and 1×10^{22} Pa s. Both KL98 and ICE-5G were used as ice models. For the simulated velocity fields the best fit model was determined based on the 3D WRMS. This procedure was repeated 2000 times for each of the three test cases. Based on this we examined how often our best fit GIA model was preferred and how often other models were preferred.

The three "true" velocity fields were as follows: (1) Our best fit GIA model (lithospheric thickness of 140 km, upper mantle viscosity of 7×10^{20} Pa s, lower mantle viscosity of 4×10^{21} Pa s, and KL98 ice model.), (2) our best fit GIA model but added "deformation" in the MN region (see Figure 4), and (3) our observed velocity field in ITRF2008. Velocity field (1) reflects a situation where all the "true" deformations in our region are the deformations included in the GIA model, the only uncertainties are the ones that are due to uncertainties in the GPS system and the GPS analysis itself. Velocity field (2) reflects a situation where all deformations in our region are the deformations included in the GIA model except some "neotectonic" signal in the MN region. In *Olesen et al.* [2013], neotectonic deformations in the NE region at the 1 mm/yr level are revealed based on GPS campaign measurements and InSAR. We have therefore added "neotectonic" deformation based on a normal distribution with standard deviation equal to 1 mm/yr and zero mean. Velocity field (3) reflects a situation with all the different deformations we actually have in the region included in the velocity field, for instance, neotectonic, monument instability, and GIA signals not included in our 1D GIA models.

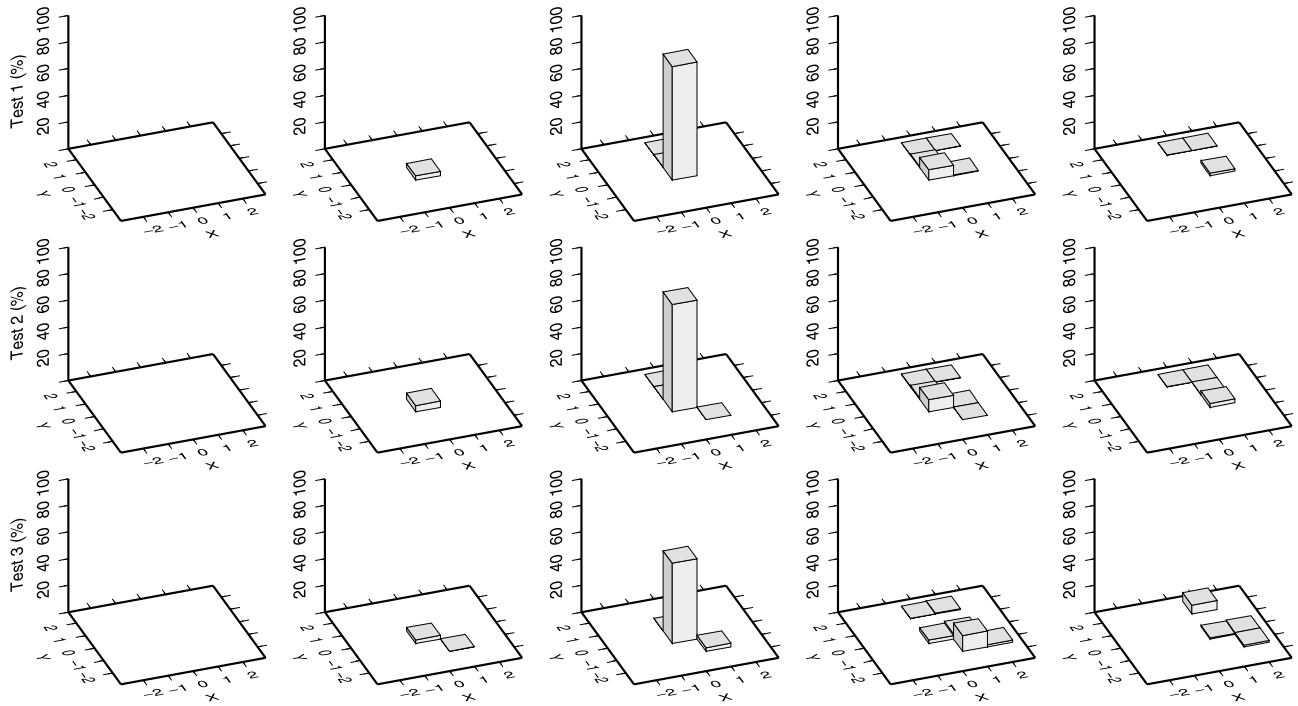

Figure 10. Validation of the GIA frame approach.The *Z* axis is the percentage of simulations that prefer the different GIA models for the three test cases described in the text. The lithospheric thickness varies from the left (120 km) to the right (160 km) in 10 km steps. *X* axis is upper mantle viscosity; −2 (2×10^{20} Pa s), −1 (4×10^{20} Pa s), 0 (7×10^{20} Pa s), 1 (1×10^{21} Pa s), and 2 (2×10^{21} Pa s). *Y* axis is lower mantle viscosity; −2 (1×10^{21} Pa s), −1 (2×10^{21} Pa s), 0 (4×10^{21} Pa s), 1 (7×10^{21} Pa s), and 2 (1×10^{22} Pa s). That is, the *X* and *Y* axis annotation indicates steps from our preferred GIA model. The ice model is KL98 in all cases (only 3.3% of the simulations for Test 3 prefer GIA models with the ICE-5G ice model. No simulation for Test 1 or Test 2 prefers GIA models with ICE-5G.) Note: This is based on the 3D WRMS.

The outcome of the simulations is plotted in Figure 10. In test case (1) 85.2% of the samples identified the best model and more than 96% found the correct viscosity parameters. None of the samples preferred the ICE-5G model. In test case (2) 80.5% identified the best fitting model and more than 94% gave the correct viscosity parameters. This indicates that the method is quite robust for neotectonic or other deformations in a limited area. In test case (3) the percentage of samples that identified our best fitting model were 61.1%. We attribute this lower number to the fact that we have ongoing deformations in Fennoscandia measured by GPS but not included in our GIA models (i.e., neotectonic, monument instability, and/or GIA signals not included in our 1D GIA models). Nevertheless, we find this relative high number as an indication that the GIA frame approach is robust. Among the simulations in Test 3 only 15.3% identified a GIA model where the Earth parameters were shifted two steps (see Figure 10). Only 3.3% preferred the ICE-5G ice history.

9. Discussion

The WRMS results using the GIA frame approach give us almost the same Earth parameters for the best fitting model independently if we look at the horizontal or vertical component. This strongly supports the GIA frame approach as being appropriate for evaluating GIA models, without introducing unnecessary constraints that may distort the results.

The best fitting KL98-NMM GIA model generally performs better than the best fitting ICE-5G-NMM GIA model. In the northeast of the study area (north of 62°N and east of 20°E), ICE-5G-NMM overpredicts the uplift, while KL98-NMM overpredicts the uplift in mid-Norway.

We find that the 1D Earth models provide better fit to the data than those models which include lateral heterogeneities. This is not surprising as both the ICE-5G and KL98 ice-load histories were constructed using a 1D Earth model. However, in the two problematic areas, the northeast for ICE-5G-NMM and mid-Norway for KL98-NMM, the 3D models perform better. This indicates that the problem in these areas might be due to lateral inhomogeneities in the lithosphere and mantle. However, we also note that the 3D model used does not include compressibility fully. Incompressible models usually give about 20 to 25% smaller velocities

than compressible models [*Tanaka et al.*, 2011], which explains the good fit of the 3D GIA models in the problematic areas of the 1D GIA models.

The Norwegian area between 65° and 68° N, has larger horizontal residuals than the rest of the network. This area is known to have large neotectonic activity [*Olesen et al.*, 2013]. Moreover, the observation time for most of the stations in this area is shorter than for the rest of the network, and thus we presume larger uncertainties here than for the rest of the network. Hence, a more detailed analysis has to be postponed until the observation time has increased sufficiently so that more reliable velocities can be determined from the data.

Atmospheric loading and hydrological loading are not modeled in the analysis. Such loadings have an effect on seasonal signals and the measurement noise, but since all the stations have at least 3 years of data (most of them have in fact much more), seasonal loading effects will not have a large influence on the secular velocities [e.g., *Blewitt and Lavallée*, 2002]. *van Dam et al.* [2001] found that the GPS trend caused by water storage loading decreases as the length of the observing period increases; the trend decreases at all sites from greater than 5 mm/yr after 1 year of data to less than 0.3 mm/yr after 20 years. They also showed that the trend of vertical displacement with 3 years of water storage loading gives around −1.5 mm/yr in Fennoscandia. In a more recent study, *Wang et al.* [2013] found with a simulation test that large scale hydrology as calculated from a global hydrology model would affect GPS trends only within the error bars of current GPS trend estimates from up to 10 years of data. The hydrological effect on the GPS-derived trend in Fennoscandia is at most 0.3 mm/yr after 8.5 years. Nontidal ocean loading might have a quasi-secular signal especially close to the Baltic Sea [see *Nordman et al.*, 2009].

In section 6 we examine the transformation parameters between ITRF2008 and the GIA reference frames. The transformation parameters from ITRF2008 to our results using the GIA frame approach, give the rigid rotation of Eurasia not contaminated by the processes included in the GIA model. In principle, the transformation parameters from ITRF2008 and the GIA reference frame also give constraints on the scale rate. However, we see how small perturbations of the upper or lower mantle viscosity give large variations in the scale rate of the system making it difficult to precisely constrain the scale rate parameter with the GIA models.

In section 7 the differences between the GIA frame approach and the traditional approach (where the reference frame is fixed and the rigid rotation is removed) are examined. The traditional approach narrows the sample of reliable GIA models, i.e., if the scale, rotation, and geocenter of the reference frame are correctly and independently estimated, the traditional approach gives better constraints on the Earth model. However, we also see how another acceptable selection of reference frames (ITRF2000) or rigid rotation (BA11) could affect the best fitting Earth model by preferring completely different models. Both scale rate, rotation, and geocenter motion have been studied in detail earlier [*Argus*, 2007; *Argus et al.*, 2011; *Blewitt*, 2003; *Wu et al.*, 2011] with different results. Differences can be caused by insufficiencies in the geodetic network or geodetic analysis strategies, inappropriate selection of reference frame, unmodeled or inadequately modeled geophysical processes, and/or poor separation of different processes. As long as we have unanswered questions regarding the reference frame realization or the rigid rotation, the traditional approach might provide incorrect constraints on GIA models. The GIA frame approach avoids these problems related to rigid rotation, scale, and/or geocenter motion. On the other hand, the GIA frame approach introduces more degrees of freedom and might increase the uncertainty and mask any large scale systematic GIA model biases. Our Monte Carlo tests reveal that our approach is robust in this regard as different models of ice history are correctly identified at the 97% level. However, depending on deformation patterns, the identified Earth model may be slightly biased in almost 40% of cases.

10. Conclusions

We introduced a new 3D velocity field for northern Europe based on GPS observation at 150 stations. The velocity field clearly shows the apparent GIA signature with a maximal uplift rate of about 10.2 mm/yr in the center. Horizontal velocities show an outward movement of the crust from this center to the so-called hinge line (the area of no vertical movement) with largest values at mid-distance. We successfully realize this new GPS velocity field directly in the so-called GIA reference frames (Note: This is an approximation to a reference frame with origin in the CE and corotating with the Eurasian plate). Hence, we avoid skewed results due to uncertainties in the reference frame or wrongly determined rigid rotation. The GIA reference

frame is enabled by the velocities determined by the GIA models. We tested several different but commonly used GIA models.

The best fitting 1D Earth model together with the ice load history used in former BIFROST studies (KL98) has a lithospheric thickness of 140 km (120–160 km within σ_1 uncertainty), an upper mantle viscosity of 7×10^{20} Pa s ($(5–20) \times 10^{20}$ Pa s), and a lower mantle viscosity of 4×10^{21} Pa s ($(3–50]) \times 10^{21}$ Pa s). Using the ICE-5G ice model, the best fitting 1D Earth model has the same lithospheric thickness and upper mantle viscosity, but a slightly lower lower mantle viscosity of 2×10^{21} Pa s. However, we note that the GPS observations, as many other GIA observations, have limitations in determining the lower mantle viscosity [*Steffen and Wu*, 2011]. We also note that earlier inferences of lower mantle viscosity may have been biased by the reference frame. Mantle viscosities are comparable to those in previous studies using BIFROST velocity estimates, whereas the lithospheric thickness is slightly higher (140 versus 120 km, see Table 3 in *Steffen and Wu* [2011]). Three-dimensional GIA models perform satisfactorily for the KL98 and ICE-5G ice histories, but not as well as the best fitting 1D GIA models.

The best fitting KL98-NMM model has WRMS of the residuals in up, 2D horizontal, and 3D of 0.42 mm/yr, 0.52 mm/yr, and 0.67 mm/yr, respectively. This implies that the existing GIA model can explain crustal movements at approximately the 0.5 mm/yr level (1 sigma). The remaining signal can be due to the GPS analysis, measurements noise, unstable monuments, deficiencies in the GIA models, or other geophysical processes.

With the GIA frame approach we can determine the rigid rotation of Eurasia relative to ITRF2008 where the modeled GIA signal is removed. However, errors in the GIA model and/or other geophysical processes might be absorbed in the transformation parameters. For the best fitting GIA model, we get a rotation vector for Eurasia of (0.103 mas/yr, 0.515 mas/yr, −0.742 mas/yr), which is in relatively close agreement with *Altamimi et al.* [2012]. Due to large correlation between mantle viscosity and scale rate, we are not able to place reliable constraints on the scale rate.

Acknowledgments
We would like to thank Matt King, an anonymous reviewer, and the editors for their comments that greatly helped in improving the manuscript. We would also like to acknowledge Bob King for his valuable inputs regarding the GAMIT/GLOBK processing. Hansheng Wang is supported by National Natural Science Foundation of China (grants 41021003 and 41174016) and CAS/SAFEA International Partnership Program for Creative Research Teams. Figures were drawn using the Generic Mapping Tools [*Wessel and Smith*, 1998].

References

Altamimi, Z., X. Collilieux, J. Legrand, B. Garayt, and C. Boucher (2007), ITRF2005: A new release of the international terrestrial reference frame based on time series of station positions and earth orientation parameters, *J. Geophys. Res.*, *112*, B09401, doi:10.1029/2007JB004949.

Altamimi, Z., X. Collilieux, and L. Métivier (2011), ITRF2008: An improved solution of the international terrestrial reference frame, *J. Geod.*, *85*, 457–473, doi:10.1007/s00190-011-0444-4.

Altamimi, Z., L. Metivier, and X. Collilieux (2012), ITRF2008 plate motion model, *J. Geophys. Res.*, *117*, B07402, doi:10.1029/2011JB008930.

Argus, D. F., R. G. Gordon, and C. DeMets (2011), Geologically current motion of 56 plates relative to the no-net-rotation reference frame, *Geochem. Geophys. Geosyst.*, *12*, Q11001, doi:10.1029/2011GC003751.

Argus, F. A. (2007), Defining the translation velocity of the reference frame of Earth, *Geophys. J. Int.*, *169*(3), 830–838, doi:10.1111/j.1365-246X.2007.03344.x.

Argus, F. A. (2012), Uncertainty in the velocity between the mass center and surface of Earth, *J. Geophys. Res.*, *117*, B10405, doi:10.1029/2012JB009196.

Blewitt, G. (2003), Self-consistency in reference frames, geocenter definition, and surface loading on the solid Earth, *J. Geophys. Res.*, *108*(B2), 2103, doi:10.1029/2002JB002082.

Blewitt, G., and D. Lavallée (2002), Effect of annual signals on geodetic velocities, *J. Geophys. Res.*, *107*(B7), 2156–2202, doi:10.1029/2001JB000570.

Boehm, J., B. Werl, and H. Schuh (2006), Troposphere mapping functions for GPS and very long baseline interferometry from European Centre for Medium-Range Weather Forecasts operational analysis data, *J. Geophys. Res.*, *111*, B02406, doi:10.1029/2005JB003629.

Boucher, C., and Z. Altamimi (2011), *Memo: Specifications for Reference Frame Fixing in the Analysis of a EUREF GPS Campaign, Ver. 8.* [Available at http://etrs89.ensg.ign.fr/.]

Ekström, G., and A. M. Dziewonski (1998), The unique anisotropy of the Pacific upper mantle, *Nature*, *394*, 168–172, doi:10.1038/28148.

Farrell, W. E., and J. A. Clark (1976), On postglacial sea level, *Geophys. J. R. Astron. Soc.*, *46*, 647–667, doi:10.1111/j.1365-246X.1976.tb01252.x.

Grand, S. P., R. D. Van Der Hilst, and S. Widiyantoro (1997), Global seismic tomography: A snapshot of convection in the Earth, *Geol. Soc. Am.*, *7*(4), 1–7.

Herring, T., R. King, and S. McClusky (2011), Introduction to GAMIT/GLOBK release 10.4, *Tech. Rep.*, Mass Inst. of Technol., Cambridge, U. K.

Hill, E. M., J. L. Davis, M. E. Tamisiea, and M. Lidberg (2010), Combination of geodetic observations and models for glacial isostatic adjustment fields in Fennoscandia, *J. Geophys. Res.*, *115*, B07403, doi:10.1029/2009JB006967.

Ivins, E. R., and C. G. Sammis (1995), On lateral viscosity contrast in the mantle and the rheology of low frequency geodynamics, *Geophys. J. Int.*, *123*, 305–322, doi:10.1111/j.1365-246X.1995.tb06856.x.

Johansson, J., et al. (2002), Continous GPS measurements of postglacial adjustment in Fennoscandia 1. Geodetic result, *J. Geophys. Res.*, *107*(B8), 2157, doi:10.1029/2001JB000400.

Khan, S. A., J. Wahr, L. A. Stearns, G. S. Hamilton, T. Van Dam, K. M. Larson, and O. Francis (2007), Elastic uplift in southeast Greenland due to rapid ice mass loss, *Geophys. Res. Lett.*, *34*, L21701, doi:10.1029/2007GL031468.

Kierulf, H. P., H. P. Plag, and O. Kristiansen (2003), Towards the true rotation of a rigid Eurasia, in *EUREF Publication No. 12, Mitteilungen des Bundesamtes für Kartografie und Geodäsie*, edited by J. A. Torres, and H. Hornik, pp. 118–124, Verlag des Bundesamtes für Kartographie und Geodäsie, Frankfurt am Main.

Kierulf, H. P., H. P. Plag, and J. Kohler (2009), Measuring surface deformation induced by present-day ice melting in Svalbard, *Geophys. J. Int.*, *179*(1), 1–13, doi:10.1111/j.1365-246X.2009.04322.x.
Kierulf, H. P., M. Ouassou, M. J. R. Simpson, and O. Vestøl (2012), A continuous velocity field for Norway, *J. Geod.*, *87*, 337–349, doi:10.1007/s00190-012-0603-2.
King, M., et al. (2010), Improved constraints on models of glacial isostatic adjustment: A review of the contribution of ground-based geodetic observations, *Surv. Geophys.*, *31*, 465–507, doi:10.1007/s10712-010-9100-4.
Lambeck, K., C. Smither, and P. Johnston (1998), Sea-level change, glacial rebound and mantle viscosity for Northern Europe, *Geophys. J. Int.*, *134*, 102–144, doi:10.1046/j.1365-246x.1998.00541.x.
Lidberg, M., J. Johansson, H. G. Scherneck, and J. Davis (2007), An improved and extended GPS-derived velocity field for the glacial isostatic adjustment in Fennoscandia, *J. Geod.*, *81*(3), 213–230, doi:10.1007/s00190-006-0102-4.
Lidberg, M., J. M. Johansson, H. G. Scherneck, and G. A. Milne (2010), Recent results based on continuous GPS observations of the GIA process in Fennoscandia from BIFROST, *J. Geodyn.*, *50*(1), 8–18, doi:10.1016/j.jog.2009.11.010.
Milne, G., J. Davis, J. Mitrovica, H. G. Scherneck, J. Johansson, M. Vermeer, and H. Koivula (2001), Space-geodetic constraints on glacial isostatic adjustments in Fennoscandia, *Science*, *291*(5512), 2381–2385, doi:10.1126/science.1057022.
Milne, G. A., J. X. Mitrovica, H. G. Scherneck, J. L. Davis, and J. M. Johansson (2004), Continuous GPS measurements of postglacial adjustment in Fennoscandia: 2. Modeling results, *J. Geophys. Res.*, *109*, B02412, doi:10.1029/2003JB002619.
Mitrovica, J. X., J. L. Davis, and I. I. Shapiro (1994), A spectral formalism for computing three-dimensional deformations due to surface load, 2. Present-day glacial isostatic adjustment, *J. Geophys. Res.*, *99*, 7075–7101, doi:10.1029/93JB03128.
Nordman, M., J. Mäkinen, H. Virtanen, J. M. Johansson, M. Bilker-Koivula, and J. Virtanen (2009), Crustal loading in vertical GPS time series in Fennoscandia, *J. Geodyn.*, *48*(3), 144–150, doi:10.1016/j.jog.2009.09.003.
Olesen, O., H. P. Kierulf, M. Brönner, E. Dalsegg, O. Fredin, and T. Solbakk (2013), Deep weathering, neotectonics and strandflat formation in Nordland, northern Norway, *Norwegian J. Geol.*, *93*(3-4), 189–213.
Peltier, W. R. (1994), Ice age paleotopography, *Science*, *265*, 195–201, doi:10.1126/science.265.5169.195.
Peltier, W. R. (1996), Mantle viscosity and ice-age ice sheet topography, *Science*, *273*, 1359–1364, doi:10.1126/science.273.5280.1359.
Peltier, W. R. (2004), Global glacial isostasy and the surface of the iceage Earth: The Ice-5G (VM2) model and GRACE, *Annu. Rev. Earth Planet. Sci.*, *32*, 111–149, doi:10.1146/annurev.earth.32.082503.144359.
Scherneck, H. G. (1991), A parametrized solid Earth tide model and ocean tide loading effects for global geodetic baseline measurements, *Geophys. J. Int.*, *106*(3), 677–694, doi:10.1111/j.1365-246X.1991.tb06339.x.
Scherneck, H-G, J. M. Johansson, J. X. Mitrovica, and J. L. Davis (1998), The BIFROST project: GPS determined 3-D displacement rates in Fennoscandia from 800 days of continuous observations in the SWEPOS network, *Tectonophysics*, *294*, 305–321, doi:10.1016/S0040-1951(98)00108-5.
Steffen, H., and G. Kaufmann (2005), Glacial isostatic adjustment of Scandinavia and northwestern Europe and the radial viscosity structure of the Earth's mantle, *Geophys. J. Int.*, *163*(2), 801–812, doi:10.1111/j.1365-246X.2005.02740.x.
Steffen, H., and P. Wu (2011), Glacial isostatic adjustment in Fennoscandia: A review of data and modeling, *J. Geodyn.*, *52*(3-4), 169–204, doi:10.1016/j.jog.2011.03.002.
Steffen, H., and P. Wu (2014), The sensitivity of GNSS measurements in Fennoscandia to distinct three-dimensional upper-mantle structures, *Solid Earth*, *5*, 557–567, doi:10.5194/se-5-557-2014.
Steffen, H., G. Kaufmann, and P. Wu (2006), Three-dimensional finite-element modelling of the glacial isostatic adjustment in Fennoscandia, *Earth Planet Sci. Lett.*, *250*, 358–375, doi:10.1016/j.epsl.2006.08.003.
Steffen, H., P. Wu, and G. Kaufmann (2007), Sensitivity of crustal velocities in Fennoscandia to radial and lateral viscosity variations in the mantle, *Earth Planet Sci. Lett.*, *257*(3-4), 474–485, doi:10.1016/j.epsl.2007.03.002.
Tanaka, Y., V. Klemann, Z. Martinec, and R. E. M. Riva (2011), Spectral-finite element approach to viscoelastic relaxation in a spherical compressible Earth: Application to GIA modelling, *Geophys. J. Int.*, *184*, 220–234, doi:10.1111/j.1365-246X.2010.04854.x.
Teferle, F. N., et al. (2009), Crustal motions in Great Britain: Evidence from continuous GPS, absolute gravity and Holocene sea level data, *Geophys. J. Int.*, *178*, 23–46, doi:10.1111/j.1365-246X.2009.04185.x.
Tushingham, A. M., and W. R. Peltier (1991), Ice–3G: A new global model of late Pleistocene deglaciation based upon geophysical predictions of post-glacial relative sea level change, *J. Geophys. Res.*, *96*, 4497–4523, doi:10.1029/90JB01583.
van Dam, T., J. Wahr, P. C. D. Milly, A. B. Shmakin, G. Blewitt, D. Lavallee, and K. M. Larson (2001), Crustal displacements due to continental water loading, *Geophys. Res. Lett.*, *28*(4), 651–654, doi:10.1029/2000GL012120.
Wang, H., P. Wu, and W. Van der Wal (2008), Using postglacial sea level, crustal velocities and gravity-rate-of-change to constrain the influence of thermal effects on mantle lateral heterogeneities, *J. Geodyn.*, *46*(3-5), 104–117, doi:10.1016/j.jog.2008.03.003.
Wang, H., L. Jia, P. Wu, L. Jiang, H. Hsu, L. Xiang, and Z. Wang (2013), Increased water storage in North America and Scandinavia from GRACE gravity data, *Nat. Geosci.*, *6*, 38–42, doi:10.1038/ngeo1652.
Wessel, P., and W. H. F. Smith (1998), New, improved version of the generic mapping tools released, *Eos Trans. AGU*, *79*(47), 579, doi:10.1029/98EO00426.
Williams, S. D. P. (2008), CATS: GPS coordinate time series analysis software, *GPS Solutions*, *12*(2), 147–153, doi:10.1007/s10291-10007-10086-10294.
Williams, S. D. P., Y. Bock, P. Fang, P. Jamason, R. M. Nikolaidis, L. Prawirodirdjo, M. Miller, and D. J. Johnson (2004), Error analysis of continuous GPS position time series, *J. Geophys. Res.*, *109*, 1–19, doi:10.1029/2003JB002741.
Wu, P. (1978), Response of a Maxwell Earth to applied surface mass loads: Glacial isostatic adjustment, MS thesis, Department of Physics, Univ. of Toronto.
Wu, P. (2004), Using commercial finite element packages for the study of Earth deformations, sea levels and the state of stress, *Geophys. J. Int.*, *158*(2), 401–408, doi:10.1111/j.1365-246X.2004.02338.x.
Wu, P., H. Wang, and H. Steffen (2013), The role of thermal effect on mantle seismic anomalies under Laurentia and Fennoscandia from observations of Glacial Isostatic Adjustment, *Geophys. J. Int.*, *192*, 7–17, doi:10.1093/gji/ggs009.
Wu, X., X. Collilieux, Z. Altamimi, B. Vermeersen, R. Gross, and I. Fukumori (2011), Accuracy of the international terrestrial reference frame origin and Earth expansion, *Geophys. Res. Lett.*, *38*, L13304, doi:10.1029/2011GL047450.
Zhao, S., K. Lambeck, and M. Lidberg (2012), Lithosphere thickness and mantle viscosity inverted from GPS-derived deformation rates in Fennoscandia, *Geophys. J. Int.*, *190*(1), 278–292, doi:10.1111/j.1365-246X.2012.05454.x.